Title No. 119-S59

Quantifying Material Uncertainty in Seismic Evaluations of Reinforced Concrete Bridge Column Structures

by Christopher L. Segura Jr., Siamak Sattar, and Mohammad Amin Hariri-Ardebili

In seismic performance evaluations, the force-deformation response of a structure is typically assessed using a deterministic analytical model, and inherent uncertainty is often neglected. For reinforced concrete structures, a source of uncertainty is variability in the mechanical properties of reinforcing steel and concrete (that is, material uncertainty). This paper presents an analytical investigation to quantify the impact of the statistical variability in mechanical properties of ASTM A706 Grade 60, 80, and 100 reinforcing steel and normalweight concrete on the seismic response of reinforced concrete bridge columns. The effects on the drift response, expressed by the coefficient of variation (COV), range between COV values of 0.1 for low-to-moderate ductility demands (that is, drift ratio < 5%), and 0.3 for larger ductility demands. The COV of the force demand is lower, ranging between 0.05 and 0.1. Overall, the study shows that material uncertainty can be incorporated in seismic performance assessments through a few additional analyses.

Keywords: endurance time analysis; Latin hypercube sampling; materials; performance-based earthquake engineering; reinforced concrete; seismic assessment; uncertainty.

INTRODUCTION

Uncertainty in seismic performance evaluations of structures stems from various factors, such as unpredictability in earthquake ground motion characteristics and variability in construction materials and as-built dimensions, as compared to those used in design. The uncertainty in ground motions is often addressed analytically by subjecting a structural model to multiple ground motion records (record-to-record uncertainty). The structural model is typically deterministic and cannot account for other sources of uncertainty. The performance-based earthquake engineering (PBEE) framework[1,2] provides a practical procedure to account for various sources of uncertainty that impact the seismic assessment. For reinforced concrete structures, a source of uncertainty in seismic evaluations is the inherent variability in the mechanical properties of reinforcing steel and concrete, which play an important role in the force-deformation structural response and failure mechanism.

This paper presents a methodology to quantify the uncertainty in the mechanical properties of reinforcing steel and concrete and its effect on the seismic response of a reinforced concrete bridge column structure. Specifically, the following are addressed: 1) formulation of statistical distributions for reinforcing steel and concrete material properties; 2) development and validation of an analytical model using the example of a reinforced concrete bridge column; and 3) results of the study and recommendations on how to incorporate material uncertainty in seismic performance assessments.

RESEARCH SIGNIFICANCE

Quantifying uncertainty in seismic response due to material variability is important for advancing PBEE because it provides a means to better characterize the probabilistic structural response, enables thorough risk evaluation, and improves insight about potential bias in deterministic analytical models. Evaluation of uncertainty in structural seismic performance evaluations has been discussed in publications[3-8] and seismic assessment frameworks.[9-11] However, the impact of material variability has not been examined as a separate source of statistical uncertainty through a comprehensive evaluation of the material properties that affect the nonlinear seismic response of reinforced concrete structures.

MECHANICAL PROPERTIES OF REINFORCING STEEL AND CONCRETE

Variability in key mechanical properties that describe the monotonic stress-strain relationship for Grade 60 (with specified yield strength, f_y, of 60 ksi [414 MPa]), Grade 80 (f_y = 552 MPa), and Grade 100 (f_y = 690 MPa) ASTM A706[12,13] reinforcing steel and normalweight concrete with a specified compressive strength (f_c') of 28 to 41 MPa (4 to 6 ksi) is quantified through statistical distributions and correlations. While ASTM A706-16 does not include Grade 100, requirements for Grade 100 ASTM A706 are available in ACI 318-19.[13] Idealized stress-strain curves for ASTM A706 reinforcing steel and concrete are given in Fig. 1(a) and (b), respectively. Properties of reinforcing steel that are used for nonlinear structural modeling include the yield stress (f_{ym}), elastic modulus (E_s), strain-hardening ratio (b), peak tensile strain-stress (ε_u, f_u), and fracture strain (ε_f) (Fig. 1(a)). Properties of concrete used for nonlinear structural modeling include the elastic modulus of unconfined (E_{c0}) and confined (E_{cc}) concrete, peak compressive strain-stress of unconfined (ε_{c0}, f_{c0}) and confined (ε_{cc}, f_{cc}) concrete, crushing strain of unconfined (ε_{cu0}) and confined (ε_{ccu}) concrete, tensile rupture strain-stress (ε_{t0}, f_t), and ultimate tensile strain (ε_{tu}) (Fig. 1(b)). In the assumption of the linear softening branch of the concrete relationship, ε_{ccu} can be replaced by a

ACI Structural Journal, V. 119, No. 3, May 2022.
MS No. S-2021-143.R1, doi: 10.14359/51734486, received November 12, 2021, and reviewed under Institute publication policies.

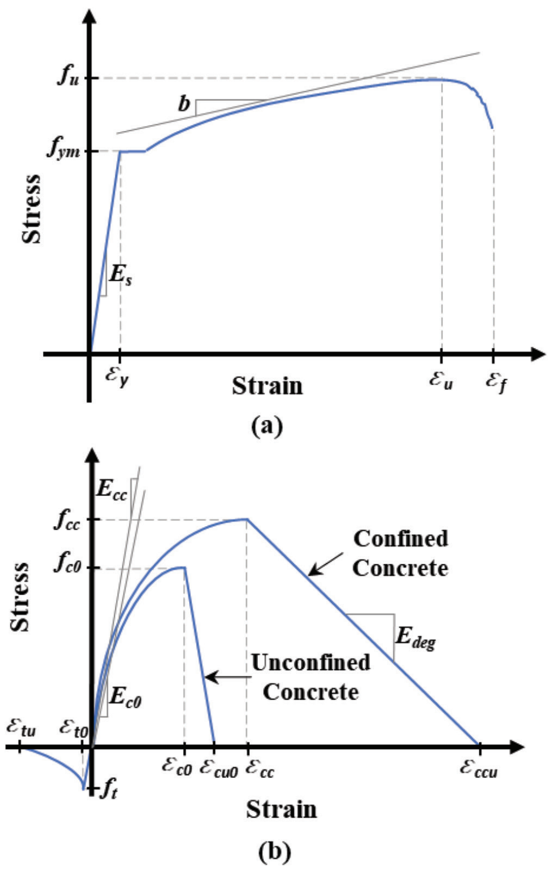

Fig. 1—Theoretical stress-strain behavior: (a) reinforcing steel in tension; and (b) concrete (compressive stress shown as positive).

softening modulus (E_{deg}). A total of 13 random variables of material properties were studied and their statistical distributions were developed, as described later. These distributions can be used to account for uncertainty in nonlinear analyses of reinforced concrete structures.

Reinforcing steel materials

Statistical distributions and correlations are developed for mechanical properties of Grade 60, 80, and 100 ASTM A706 steel reinforcement using an extensive database of test data provided to the authors courtesy of the Concrete Reinforcing Steel Institute[14] (CRSI), and data available in the literature.[15] The CRSI database includes material tests on 80,588 Grade 60 and 1419 Grade 80 ASTM A706 reinforcing bars, as well as 74 tests on bars that satisfy the ACI 318 requirements for ASTM A706 reinforcing steel.[13]

Statistical parameters (mean and coefficient of variation [COV]) for five of the mechanical properties shown in Fig. 1(a) are summarized in Table 1 for Grades 60, 80, and 100 ASTM A706 reinforcement. For each material property, uncertainty is represented by normal probability density functions selected using the Kolmogorov-Smirnov goodness-of-fit test[16] (K-S test) with a rejection p-value of 0.05. Histograms of material property values f_{ym}, f_u, ε_f, and b are presented in Fig. A1, along with the fitted normal distribution. Values of b, defined as ratio of the secant hardening modulus E_{sh} and elastic modulus E_s ($b = E_{sh}/E_s$), are determined for each CRSI material test by calculating the slope between the yield point (ε_y, f_{ym}) and the tensile strength point (ε_u, f_u), and dividing this slope by the mean value of E_s = 201,327 MPa (29,200 ksi). The point ε_u is not reported in the CRSI data. However, using stress-strain curves collected from research reports for Grade 60 and Grade 80 A706/A615 reinforcing bars, Mander and Matamoros[17] adopted a fixed value of $\varepsilon_f/\varepsilon_u = 1.2$ to relate ε_f and ε_u. Implementing the same approach, values of b for each CRSI material test are calculated as $\varepsilon_u = \varepsilon_f/1.2$, and a statistical distribution is fit to the data. It is noted that the dispersion approximated for b by this approach (COV = 19.4%) is similar to that reported in the literature for ASTM A706 reinforcing bars using smaller data sets.[17,18] The distribution for E_s is taken from Mirza and MacGregor[15] because the CRSI database does not include this information. COV values reported in Table 1 are generally the largest for Grade 60 and the smallest for Grade 100, which may be attributed to a much larger number of Grade 60 bar tests and a higher number of mills producing the Grade 60 bars. Table 2 presents correlation coefficients between the properties, determined using Spearman's correlation analysis[19] with a 95% confidence criterion. The approach in Sattar et al.[20] is adopted with no correlation between E_s and other properties for structural steel. For all three reinforcing grades, the reported values indicate moderate-to-strong correlation among the different reinforcing steel material properties.

Table 1—Statistical distributions for reinforcing steel mechanical properties

		Grade 60	Grade 80	Grade 100
f_{ym}	Mean, MPa	481.4	604.4	732.4
	COV, %	4.6	3.9	3.4
f_u	Mean, MPa	655.8	793.9	942.8
	COV, %	4.3	3.4	3.7
ε_f	Mean	0.16	0.139	0.115
	COV, %	13.6	12.7	12.8
E_s	Mean, GPa	201.3	201.3	201.3
	COV, %	3.3	3.3	3.3
b	Mean	0.0067	0.0085	0.0115
	COV, %	19.4	17.6	13

Note: 1 MPa = 0.145 ksi; 1 GPa = 145 ksi.

Table 2—Correlation coefficients for reinforcing steel mechanical properties

		Grade 60	Grade 80	Grade 100
f_{ym}	f_u	0.543	0.740	0.901
f_{ym}	ε_f	–0.266	–0.290	–0.034
f_{ym}	b	0	0.136	0.252
f_u	ε_f	–0.242	–0.348	0.077
f_u	b	0.597	0.537	0.383
ε_f	b	–0.710	–0.828	–0.706

Concrete materials

Concrete material property statistical distributions and correlations are developed using a set of cylinder compression tests collected by the authors, referred to herein as the laboratory data set, as well as data[21] and statistical parameters[22] in the literature. The laboratory data set consists of 88 cylinder tests on normalweight concrete with a specified compressive strength of f_c' = 35 MPa (5 ksi). For all 88 tests, the concrete cylinder was instrumented with an extensometer to measure deformations up to f_{c0}, enabling calculation of ε_{c0} and E_{c0}. The laboratory data set is supplemented with data digitized from 588 reported modulus of rupture tests[21] and statistical parameters for 4636 concrete cylinder tests[22] that do not include ε_{c0} and E_{c0} measurements. Table 3 provides statistical parameters for eight of the mechanical properties shown in Fig. 1(b). Histograms of the material property values, along with the normal distribution selected using the K-S test with a p-value of 0.05, are presented in Fig. A1. COV values are similar among the three specified concrete strength values, except that dispersion in unconfined and confined strength (f_{c0} and f_{cc}) is considerably lower for concrete with specified f_c' = 41 MPa (6 ksi). Correlation coefficients between the properties, determined using Spearman's correlation analysis with a 95% confidence criterion, are given in Table 4. The reported values indicate moderate-to-strong correlation among the different concrete material properties.

Table 3—Statistical distributions for concrete mechanical properties

		f_c' = 28 MPa	f_c' = 35 MPa	f_c' = 41 MPa
E_{c0}	Mean, MPa	20,029	22,394	24,532
	COV, %	11.4	11.4	11.4
f_{c0}	Mean, MPa	33.4	42.1	50.3
	COV, %	15.5	12.5	7.5
ε_{c0}	Mean	0.00246	0.00270	0.00301
	COV, %	18.7	19.3	18.6
f_t	Mean, MPa	3.6	4.1	4.8
	COV, %	21.1	19.3	18.5
E_{cc}	Mean, MPa	23,580	26,283	28,000
	COV, %	15.0	15.6	15.4
f_{cc}	Mean, MPa	44.7	53.6	62.1
	COV, %	11.9	10.2	6.3
ε_{cc}	Mean	0.00612	0.00590	0.00594
	COV, %	15.5	16.6	17.2
E_{deg}	Mean, MPa	1,037	1,355	1,640
	COV, %	17.1	14.4	10.0

Note: 1 MPa = 0.145 ksi.

Even though the laboratory data set includes measured f_{c0} values, statistical parameters for f_{c0} are taken from Nowak et al.[22] because they are derived from a larger data set that includes 4636 cylinder tests with specified concrete strengths of f_c' = 28 MPa (4 ksi) (2784 tests), f_c' = 35 MPa (5 ksi) (1722 tests), and f_c' = 41 MPa (6 ksi) (130 tests). Measured f_{c0} values from the laboratory data set are, however, used for correlation analyses because the data reported by Nowak et al.[22] only includes measured f_{c0} values. Because the curing time for the laboratory data set varied, measured f_{c0} and E_c values are adjusted to 28-day values using relationships given in ACI 209.2R-08 (Eq. (1) and (2))[23]

$$f_{c0} = f_{c0,t}\left(\frac{\alpha+\beta t}{t}\right) \tag{1}$$

$$E_{c0} = E_{c,t}\Big/\left(\frac{t}{4+0.85t}\right)^{0.5} \tag{2}$$

where t is concrete cylinder curing time; $f_{c0,t}$ and $E_{c,t}$ are the time-dependent concrete compressive strength and modulus of elasticity, respectively; and α and β are constants reflecting cement type and curing condition. It is also noted that the laboratory data set only includes concrete materials with specified strengths of f_c' = 35 MPa (5 ksi). To estimate distributions of E_{c0} and ε_{c0} for concrete materials with f_c' = 28 and 41 MPa (4 and 6 ksi), measured values from the laboratory data set are adjusted to be representative of materials with these specified strengths. Unconfined concrete modulus of elasticity values are estimated ($E_{c0,est}$) according to Eq. (3) using the ACI 318 equation for modulus of elasticity (ACI 318-19 Eq. (19.2.2.1.b))

$$E_{c0,est} = E_{c0}\left(\frac{\sqrt{f'_{c,target}}}{\sqrt{35\text{ MPa}}}\right) \tag{3}$$

where E_{c0} is the measured values from the laboratory data set; and $f_c'_{,target}$ is the targeted value of f_c' in MPa units. The denominator of Eq. (3) represents the mean value of E_{c0} for concrete with f_c' = 35 MPa (5 ksi), and the numerator represents E_{c0} for concrete with a different f_c' value. Unconfined concrete peak compressive strain values are estimated

Table 4—Correlation matrix for concrete mechanical properties (f_c' = 35 MPa [5 ksi])

	E_{c0}	f_{c0}	ε_{c0}	f_t	E_{cc}	f_{cc}	ε_{cc}	E_{deg}
E_{c0}	1	0.224	–0.476	0	0.565	0.166	–0.304	–0.217
f_{c0}	0.224	1	0.590	0	0.078	0.822	0.146	–0.403
ε_{c0}	–0.476	0.590	1	0	–0.434	0.486	0.450	–0.060
f_t	0	0	0	1	0	0	0	0
E_{cc}	0.565	0.078	–0.434	0	1	–0.147	–0.494	–0.470
f_{cc}	0.166	0.822	0.486	0	–0.147	1	0.569	–0.456
ε_{cc}	–0.304	0.146	0.450	0	–0.494	0.569	1	–0.071
E_{deg}	–0.217	–0.403	–0.060	0	–0.470	–0.456	–0.071	1

($\varepsilon_{c0,est}$) using the concrete stress (f_c) versus concrete strain (ε_c) relationship proposed by Popovics[24] (Eq. (4a)), specifically through the parameter η, which controls the slope of the ascending branch of the curve. To do so, η is first calculated according to Eq. (4b) using measured f_{c0}, ε_{c0}, and E_{c0} values from the laboratory data set. Assuming η is constant, $\varepsilon_{c0,est}$ is then calculated by Eq. (4b) by substituting the estimated concrete strength and modulus of elasticity values (that is, $f_{c0,est}$ and $E_{c0,est}$) for f_{c0} and E_{c0}, respectively.

$$f_c = \frac{f_{c0}\left(\varepsilon_c/\varepsilon_{c0}\right)\eta}{\eta - 1 + \left(\varepsilon_c/\varepsilon_{c0}\right)^{\eta}} \tag{4a}$$

$$\eta = \frac{E_{c0}}{E_{c0} - f_{c0}/\varepsilon_{c0}} \tag{4b}$$

Using Eq. (3) and (4) could potentially introduce higher uncertainty in statistical distributions for E_{c0} and ε_{c0}. Additional material testing could improve or verify the distributions used herein.

Statistical distributions for f_t are fit to data digitized from modulus of rupture tests reported by Mirza et al.[21] (Fig. A1). Data is not available to develop statistical distributions for ε_{cu0} and ε_{tu}. In the absence of data, a commonly used assumption of $\varepsilon_{cu0} = 0.005$ is made. To calculate ε_{tu}, the softening branch of the concrete tensile response (Fig. 1(b)) is assumed to follow the relationship proposed by Kaklauskas and Ghaboussi.[25]

Statistical distributions for confined concrete properties are not easily derived from test data because there are several interrelated variables that contribute to the confined behavior (for example, confining steel yield strength and unconfined concrete strength). However, confinement models available in the literature are derived using test data that account for the variables. Uncertainty exists in the models themselves because the variables used to derive a model likely do not cover the entire probable design space and because there is dispersion in the data used. Logic tree analysis is commonly used in the earthquake engineering field to address uncertainty in seismic hazard[26,27] and force-deformation response.[28]

In this study, the logic tree approach is adopted to quantify variability in confined concrete properties for a circular bridge column, introduced later for uncertainty quantification, using four known confinement models.[29-32] A Monte Carlo simulation is employed to sample 100,000 combinations of confinement model inputs (for example, f_{c0}, ε_{c0}, f_y, and so on) based on the distributions reported in Tables 1 through 4. Using the 100,000 model input combinations, confined properties E_{cc}, f_{cc}, ε_{cc}, and E_{deg} (Fig. 1(b)) are calculated according to each of the four models. A weight factor ($w_{i,j}$) is applied to the confined property value calculated using each model (for example, $w_{i,j}f_{cc,j}$) to reflect the confidence to predict that property. Equation (5) is used to determine the weighted properties

$$\begin{aligned} E_{cc} &= \sum w_{1,j} E_{cc,j} \\ f_{cc} &= \sum w_{2,j} f_{cc,j} \\ \varepsilon_{cc} &= \sum w_{3,j} \varepsilon_{cc,j} \\ E_{deg} &= \sum w_{4,j} E_{deg,j} \end{aligned} \tag{5}$$

where $w_{i,j}$ is the weight assigned to model j (j = 1 to 4) for confined property i (i = 1 to 4); and $E_{cc,j}$, $f_{cc,j}$, $\varepsilon_{cc,j}$, and $E_{deg,j}$ are the confined properties calculated using model j. Individual confinement model outputs were compared to evaluate the confidence in the estimated circular bridge column confined properties estimated by each model. It was observed that the model proposed by Scott et al.[29] generally predicts smaller mean values for f_{cc} and ε_{cc} than the other three models, which is attributed to the fact that the model was developed using data from tests on rectangular columns, which typically demonstrate inferior confined behavior to circular sections. The models proposed by Mander et al.[30] and Légeron and Paultre[32] were observed to produce mean E_{cc} values smaller than the mean E_{c0} in Table 3, which may be attributed to the definition of E_{c0} (that is, secant or tangent modulus) used. This observation contradicts the trend identified by other researchers,[33] and used in ACI 318,[13] that the modulus of elasticity increases with increasing strength (that is, $f_{cc} > f_{c0}$). To eliminate extraneous dispersion associated with these observations, w = 0.1 (that is, low confidence) is assigned to the Scott et al. model for calculating f_{cc} and ε_{cc} and to the Légeron and Paultre and Mander et al. models to calculate E_{cc}, and equal weight factors are applied to the other models. Histograms for E_{cc}, f_{cc}, ε_{cc}, and E_{deg} are presented in Fig. A1, and fitted statistical distributions and correlation coefficients are reported in Tables 3 and 4.

MATERIAL UNCERTAINTY QUANTIFICATION

Model development and validation

To quantify the impact of material uncertainty on seismic performance evaluations, an analytical model representing the column designed according to the 2006 Caltrans Seismic Design Criteria[34] and tested on the shake table of the University of California, San Diego (UCSD) in September 2010[35] is developed. The bridge column is selected because: 1) it is a simple structure that enables a detailed evaluation of uncertainty at the component level; and 2) comprehensive experimental data are available to validate the analytical model.

A schematic of the test structure is shown in Fig. 2(a), with the structure consisting of a 1219 mm (48 in.) diameter and 7315 mm (288 in.) long column supported by a footing that was used to attach the specimen to the shake table. A large concrete block weighing 2322 kN (522,000 lb) was attached to the top of the column to simulate the weight of the bridge superstructure. Column longitudinal (flexural) reinforcement consisted of 18 No. 11 (d_b = 36 mm [1.41 in.]) Grade 60 ASTM A706 bars spaced concentrically around the perimeter of the column. Transverse reinforcement consisted of two bundled No. 5 (d_b = 16 mm [0.625 in.]) hoops spaced at 152 mm (6 in.) on center over the full height of the column.

A distributed plasticity (fiber) model of the bridge column is developed (Fig. 2(b)) and nonlinear analyses are conducted in OpenSees.[36] A fiber element formulation

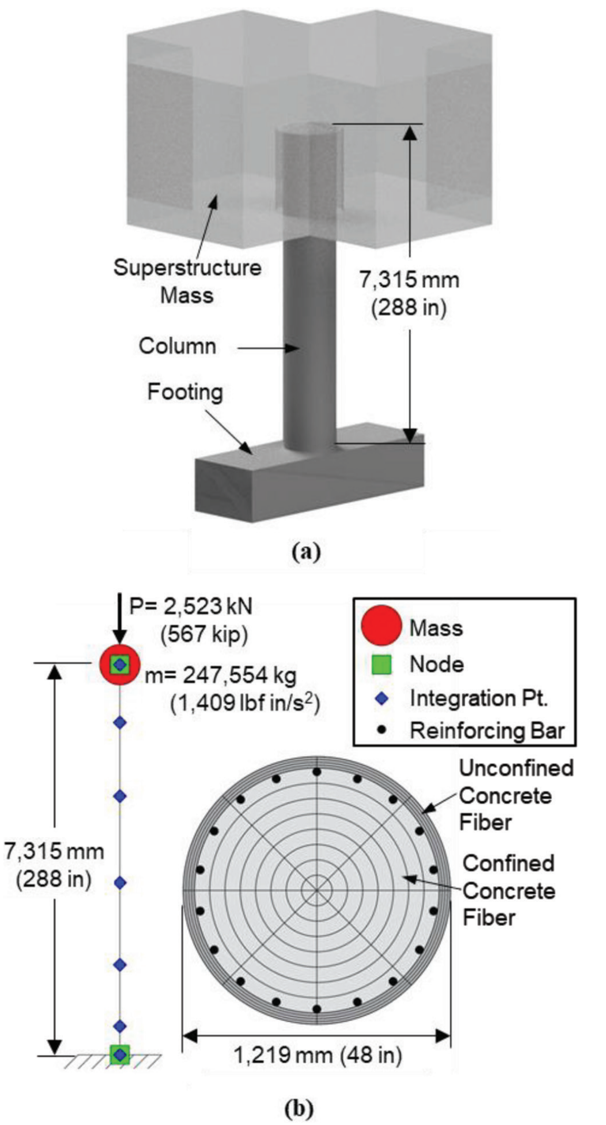

Fig. 2—(a) Bridge column specimen; and (b) analytical model discretization.

is selected because it enables direct definition of concrete and reinforcing steel mechanical properties, thereby making it possible to isolate their impact on uncertainty in seismic response parameters of the column. The model consists of a single force-based fiber element with seven Gauss-Radau integration points.[37] The cross section is discretized into 64 confined concrete fibers, 32 unconfined concrete fibers, and 18 steel reinforcing bar fibers. A lumped mass of 247,554 kg (1409 lbf s^s/in.) is applied at the top node of the column model, accounting for the mass of the superstructure and one-half the mass of the column. An axial force of 2522 kN (567,000 lbf), representing the total combined weight of the superstructure and the column, is also applied at the top node of the column and held constant throughout the analyses. Second-order P-Delta effects are accounted for in the nonlinear analyses.

Concrete stress-strain behavior is simulated using the model proposed by Chang and Mander[38] and steel reinforcing bar behavior is simulated using the model proposed by Menegotto and Pinto.[39,40] These two models employ

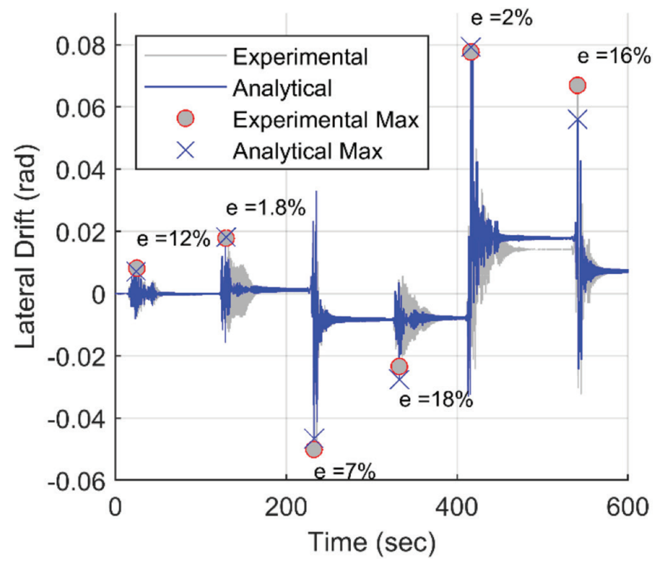

Fig. 3—Analytical model validation. (Note: Error, e, in analytical maximum values is reported for six acceleration records applied on UCSD shake table.)

sophisticated uniaxial constitutive hysteretic rules, valuable for modeling the nonlinear behavior of concrete and reinforcing steel. Regularization of inelastic material properties is conducted in accordance with the technique developed by Coleman and Spacone.[41] This technique adjusts the material stress-strain curve such that analytical results are insensitive to model spatial discretization. A tension strain limit is applied to the reinforcing bar material model to simulate bar fracture when a reinforcing bar reaches a strain equal to ε_f, and a compression strain limit is applied to simulate bar buckling by signaling the reinforcing bar model to degrade to zero stress when the confined concrete reaches ε_{ccu} (that is, confined concrete crushing). A damping coefficient of 2.5% is applied to the structural model, consistent with dynamic properties reported during shake-table testing.[35]

Model validation is conducted by comparing the response of the analytical model to the response measured experimentally on the UCSD shake table. Reported test day mechanical properties of reinforcing steel and unconfined concrete[35] and confined concrete properties determined using the method of the previous section are assigned to the analytical model. The model is then subjected to the six acceleration time histories applied during the UCSD shake-table test.[35] A comparison of the analytical and experimental lateral drift ratio at the top of the column is shown in Fig. 3. For each earthquake record, the maximum analytical and experimental drift ratio are indicated. The analytical model captures the general deformation response of the bridge column, including residual inelastic deformations. The error in the maximum predicted drift ratio (*e*), as compared to the experimental maximum value, is also indicated for each earthquake record. Error values range between 2 and 18%.

Analytical investigation

Uncertainty in the seismic response of the bridge column structure due to material variability is quantified using the validated analytical model (Fig. 2(b)) and varying the

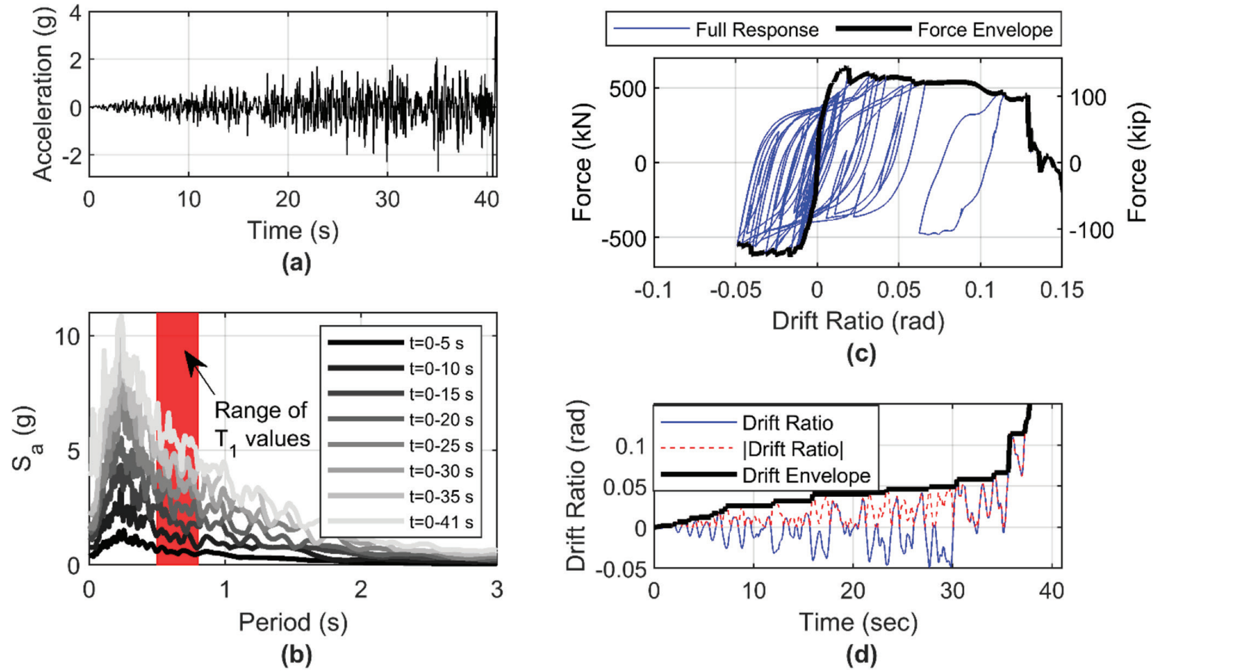

Fig. 4—(a) ETA acceleration versus time; (b) 2.5%-damped ETA acceleration response spectra for different elapsed time intervals; (c) representative force versus drift ratio result; and (d) representative drift ratio versus time.

material properties according to the distributions reported in Tables 1 through 4. Nonlinear analyses are conducted in OpenSees using the endurance time analysis (ETA) method.[42] ETA is a dynamic analysis procedure that uses a single synthetic acceleration record that subjects the structure to increasing shaking intensities. The ETA method has been validated with respect to analytical results from conventional time-history analysis for both linear and nonlinear structural response.[43] ETA is employed for this study as an alternative to analysis procedures that use multiple earthquake records[44] and, thereby, introduce record-to-record uncertainty that is undesirable for this study aimed at isolating the impact of material uncertainty. The acceleration versus time for the ETA is shown in Fig. 4(a), and the 2.5%-damped pseudo-acceleration response spectra (S_a) are plotted in Fig. 4(b) for eight representative elapsed time intervals. As shown in Fig. 4(b), spectral acceleration demands for the ETA record increase with increasing elapsed time.

Uncertainty in seismic response is quantified as the dispersion in the column force demand and the maximum absolute value of the drift ratio, referred to herein as the drift envelope. A representative force versus lateral drift ratio response is shown in Fig. 4(c). The drift ratio versus time response for the same representative analysis is shown in Fig. 4(d), along with the drift envelope. When subjected to the ETA, the model endures multiple elastic and inelastic cycles, reaching a drift of 0.1 rad in the positive loading direction prior to the onset of strength loss (for example, 20% reduction in strength from peak force).

Sensitivity analysis

A sensitivity analysis is conducted to identify the material properties that have the largest impact on analytical results. The sensitivity of each property is evaluated by setting the value of the material property to a lower bound and upper

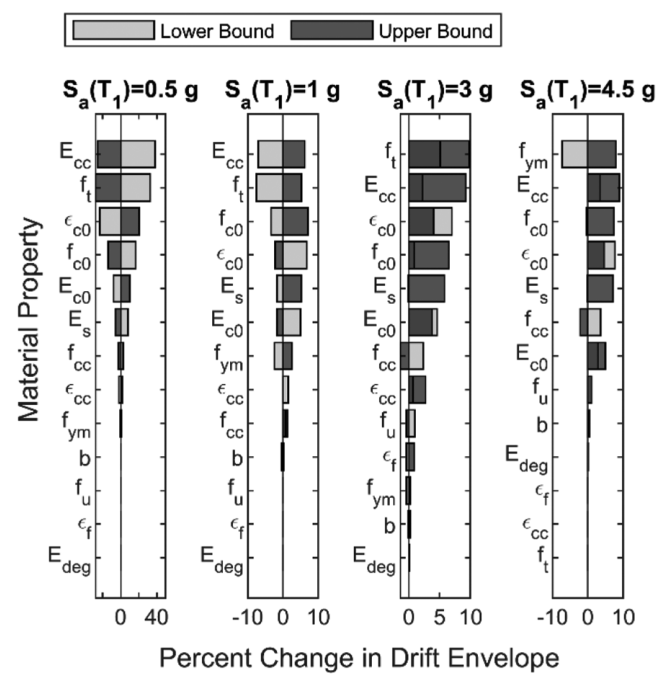

Fig. 5—Sensitivity analysis results.

bound, one at a time, while all other material properties are set at their mean values (Tables 1 and 3). Lower and upper bounds are selected as the 16th and 84th percentiles—that is, one standard deviation from the mean value (Tables 1 and 3). To quantify sensitivity, the analytical response using lower- and upper-bound properties are compared to that using mean material properties.

Figure 5 presents results of the sensitivity analysis as a tornado diagram with the vertical axis representing the 13 material properties (Tables 1 and 3) and the horizontal axis showing the sensitivity expressed as the percentage

Table 5—Characteristics of analytical model combinations

	Specified materials		Random variables		Model characteristics	
	f_c', MPa (ksi)	f_y, MPa (ksi)	N_{RV}	Deterministic variables	M_n, kN·m (ft·kip)	T_1, s
M1	35 (5)	414 (60)	13	—	4539 (3347)	0.69
M2	35 (5)	552 (80)	13	—	5412 (3991)	0.69
M3	35 (5)	690 (100)	13	—	6113 (4508)	0.69
M4	28 (4)	414 (60)	13	—	4346 (3205)	0.75
M5	41 (6)	414 (60)	13	—	4648 (3428)	0.64
M6	35 (5)	414 (60)	9	E_{deg}, f_u, ε_f, b	4539 (3347)	0.69
M7	35 (5)	414 (60)	6	E_{deg}, f_u, ε_f, b, ε_{cc}, f_{cc}, E_{c0}	4539 (3347)	0.69

difference in the drift envelope value determined at four different earthquake shaking intensities as compared to the model with all material properties set at their mean value. The shaking intensities are represented by the first mode spectral acceleration (S_a) at the fundamental period (T_1) of the bridge structure model. The period T_1 varies due to the variation in the material properties, resulting in differences in S_a. For the analyses reported herein, $S_a(T_1) = 0.5g$ represents low ductility demand ($\mu_D \approx 1.0$); $S_a(T_1) = 1g$ and $3g$ are representative of design-level ductility limits for bridges classified as Recovery (μ_D = 2.5 to 3.5) and Ordinary (μ_{Dv} = 4.0 to 5.0) according to the Caltrans Seismic Design Criteria[45]; and $S_a(T_1) = 4.5g$ represents the intensity for which the median model is expected to reach collapse-level drift demands, assumed herein as a drift ratio of 0.1 rad.

Figure 5 demonstrates that analytical results are most sensitive to material properties that define the hardening branch of the concrete stress-strain curve (for example, E_{cc}, f_{c0}, ε_{c0}, and f_t) and the elastic branch of the reinforcing steel stress-strain curve (E_s, f_{ym}). Analytical results are likely to be insensitive to E_{deg}, only marginally sensitive to b, f_u, and ε_f, and moderately sensitive to E_{c0}, f_{cc}, and ε_{cc}. Figure 5 also demonstrates that the relative importance of accounting for uncertainty in a particular property depends on the shaking intensity or performance level (for example, service, design, or near-collapse). For example, results appear to be moderately sensitive to f_{cc} at $S_a(T_1) = 3g$ and $4.5g$, but relatively insensitive to f_{cc} at smaller shaking intensity. Conversely, results are insensitive to f_t at $S_a(T_1) = 4.5g$ but very sensitive at lower intensities.

Description of analytical model combinations

Table 5 describes seven combinations of the analytical model, designated M1 through M7, that are used to quantify uncertainty in seismic response due to material variability. The model combinations differ by the choice of specified concrete and reinforcing steel strengths (that is, f_c' and f_y) used to define material property distributions, as well as the number of random material property variables (N_{RV}) included in the analyses (Table 5). The specified material properties affect the nominal flexural strength (M_n, calculated for a maximum compression strain of 0.003 according to ACI 318) and fundamental period (T_1). Model combinations M1 through M5 account for all 13 random variables (Tables 1 and 3) and make it possible to isolate the impact of the varying material properties (that is, f_c' and f_y). Model combinations M6 and M7 use fewer random variables (N_{RV} = 9 and 6, respectively), based on the sensitivity analysis (Fig. 5), to investigate the number of random variables and the minimum number of analyses needed to implement material uncertainty in seismic performance evaluations. For M1, material property distributions used for uncertainty quantification are based on f_c' = 35 MPa (5 ksi) and f_y = 414 MPa (60 ksi). M2 and M3 differ from M1 in only terms of the specified reinforcing steel strength (f_y = 552 and 690 MPa [80 and 100 ksi], respectively). M4 and M5 differ from M1 only in terms of the specified concrete strength (f_c' = 28 and 41 MPa [4 and 6 ksi], respectively). For M6, four variables (E_{deg}, f_u, ε_f, and b) are set deterministically as their mean values (N_{RV} = 9), based on the sensitivity analysis (Fig. 5). M7 is a variation of M6 with E_{c0}, ε_{cc}, and f_{cc} also set as their mean values (N_{RV} = 6).

For each model combination, 10,000 "children" models are constructed by sampling the random concrete and reinforcing steel properties in a 10,000-sample Monte Carlo simulation using the statistical distributions and correlations summarized in Tables 1 through 4. The material property sample sets are drawn from truncated distributions bounded at ±2.8 standard deviations of the mean, accounting for 99.5% of the distribution and eliminating extreme statistical outliers. For a single-model combination, the 10,000 children models differ only by the material property input values, while other modeling variables (for example, mass, damping) are held constant for all models.

Analytical results

Figure 6(a) shows force-deformation envelopes for all 10,000 children models of M1. The median (50th percentile) force value for a given drift ratio is plotted on top of the individual envelopes, along with the 5th (x_{05}), 16th (x_{16}), 84th (x_{84}), and 95th (x_{95}) percentiles of force. Figures 6(b) and (c) compare the dispersion in the column force demand, for a given drift, for all seven model combinations (that is, M1 through M7). Dispersion is determined according to Eq. (6) as the average of the 16th and 84th percentile force values normalized by the median value (x_{50}), referred to herein as average COV ($\overline{COV}$). Analogous to the definition of COV, $\overline{COV}$ accounts for the central 68% of data (that is, ±1 standard deviation) but does so explicitly by using the 16th and 84th percentile values.

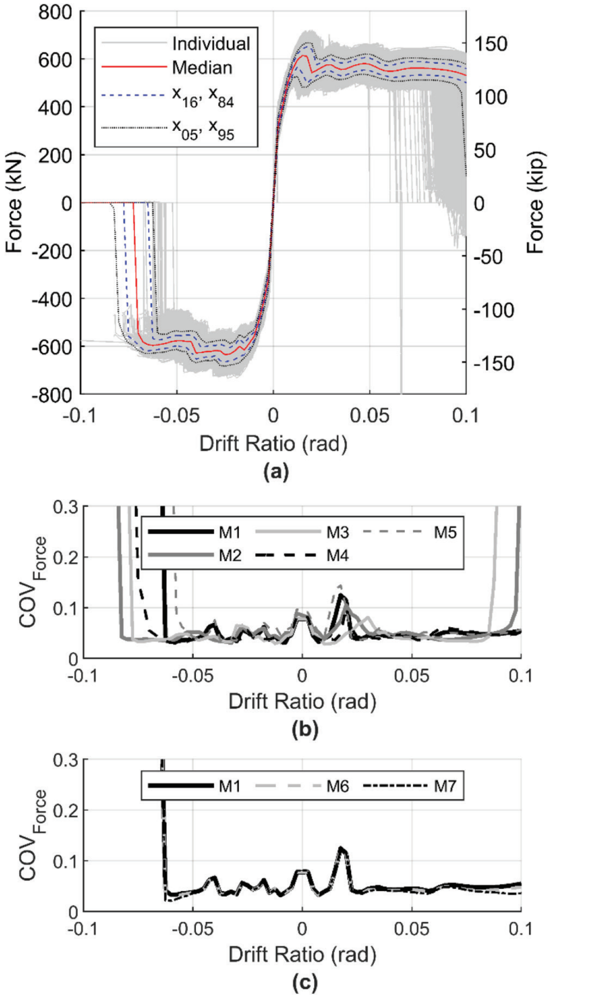

Fig. 6—(a) Model M1 force versus drift envelopes; (b) Models M1 through M5 COV of force envelope versus drift ratio; and (c) Models M1, M6, and M7 COV of force envelope versus drift ratio.

$$\overline{\mathrm{COV}} = \frac{x_{84} - x_{16}}{2x_{50}} \tag{6}$$

Prior to the onset of strength loss, the $\overline{\mathrm{COV}}$ is generally approximately 0.05 to 0.1, with all seven model combinations demonstrating similar levels of uncertainty. In comparison to other models, slightly smaller uncertainty is observed for M2 (f_y = 552 MPa [80 ksi]) and M3 (f_y = 690 MPa [100 ksi]). Figure 6(c) shows that the model combinations with fewer random variables (M6 and M7) produce nearly identical results to that of the model with 13 random variables (M1), which is discussed in more detail later.

The drift envelope response versus analysis time is plotted in Fig. 7(a) for the 10,000 M1 analyses, along with the 5th, 16th, 50th, 84th, and 95th percentile values. Drift envelope values in Fig. 7(a) are capped at 0.1 rad to account for the fact that the real structure may be expected to develop failure mechanisms that are not captured by the model at this relatively large inelastic deformation. Early in the analyses (for example, at time $t < 15$ seconds), while the models are undergoing elastic cycles or small inelastic cycles, the data are well distributed about the median. Due to the variation in T_1, some models are excited at larger shaking intensities prior to the other models, causing the data to be skewed toward larger drift values. It is appropriate, therefore, to express the dispersion using a lognormal distribution to account for the asymmetry of the distribution. Figures 7(b) and (c) compare the dispersion in drift envelope values, expressed as the lognormal standard deviation ($\sigma_{\ln X}$), calculated according to Eq. (7)[46]

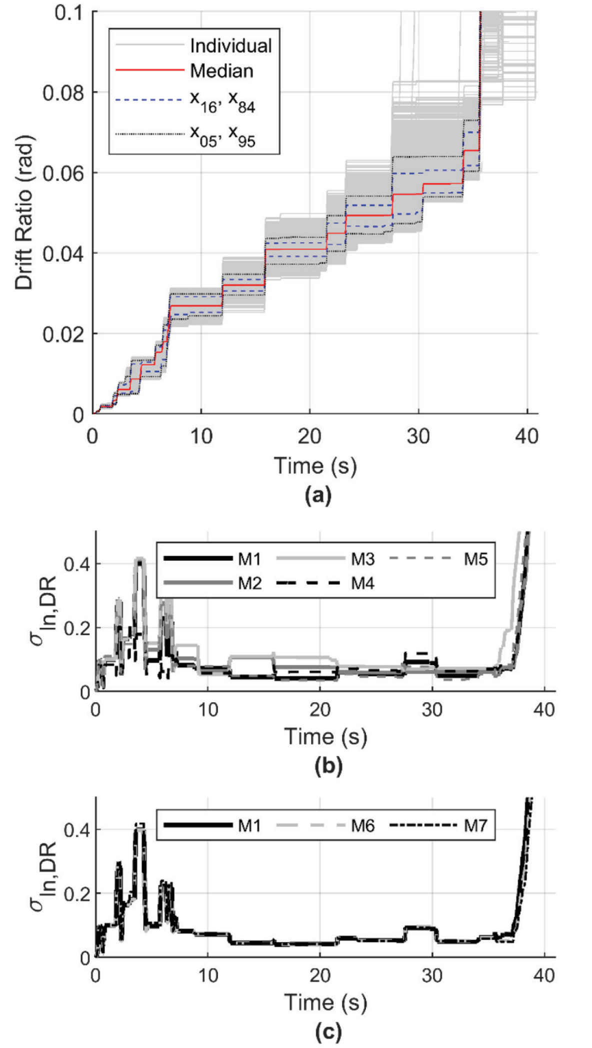

Fig. 7—(a) Model M1 drift envelopes; (b) Models M1 through M5 $\sigma_{ln,\mathrm{DR}}$ versus time; and (c) Models M1, M6, and M7 $\sigma_{ln,\mathrm{DR}}$ versus time.

$$\sigma_{\ln X} = \ln\left(\sqrt{\frac{x_{84}}{x_{16}}}\right) \tag{7}$$

$\sigma_{\ln X}$ values in Fig. 7 are generally approximately 0.05 to 0.1 prior to the onset of 20% strength loss; however, values of approximately 0.3 to 0.4 are observed early in the analyses ($t < 10$ seconds). This trend is attributed to differences in the fundamental period of the individual models (Fig. 4). The dispersion again becomes large ($\sigma_{\ln X} > 0.4$) for $t > 35$ seconds, as several models experience strength loss and approach the collapse drift limit (0.1 rad). M2 (f_y = 552 MPa [80 ksi]), M3 (f_y = 690 MPa [100 ksi]), and M4 (f_c' = 28 MPa [4 ksi]) demonstrate the largest uncertainty in Fig. 7(b) and (c). For M2 and M3, this is attributed to the development of larger internal forces and larger concrete compression strain demands than M1, caused by higher reinforcing bar tensile stresses. For M4, larger uncertainty is also attributed to the development of higher concrete compression strain demands due to lower concrete strength in this case. Figure 7(c) shows that analytical results are nearly identical when fewer random variables are used (M6 and M7) as compared to the reference model with 13 random variables (M1).

In the PBEE framework, the vulnerability of a structure to collapse is often expressed in terms of ground shaking intensity to account for differences in the excitation characteristics of structures (for example, different T_1 values). The shaking intensity measure often used is the first mode elastic spectral acceleration ($S_a(T_1)$). In Fig. 8(a), drift envelope values are plotted against $S_a(T_1)$ for M1, enabling a more direct comparison of dispersion based on the shaking intensity rather than analysis time (that is, Fig. 7), with T_1 varying for each analysis. To derive the individual values shown in Fig. 8(a), statistical parameters of the drift response (for example, x_{16} and x_{84}) are derived from drift envelope values binned in 0.25g $S_a(T_1)$ increments (for example, $S_a(T_1)$ = 1.0 to 1.25 g). Figures 8(b) and (c) present the lognormal standard deviation of the drift envelope versus $S_a(T_1)$ for all seven model combinations. A comparison of Fig. 7 and 8 indicates that larger uncertainty is introduced with the transition from the time domain to $S_a(T_1)$. This is attributed to the use of an elastic spectral value ($S_a(T_1)$) to represent earthquake shaking intensity for a structure behaving nonlinearly. When dispersion in the drift envelope is presented in terms of $S_a(T_1)$, $\sigma_{\ln X}$ values are on the order of 0.10 to 0.15 for moderate shaking intensities ($S_a(T_1) \approx 1$ to 3g) that do not lead to collapse-level drifts. At larger shaking intensities ($S_a(T_1) > 3g$), $\sigma_{\ln X}$ increases to approximately 0.3. Uncertainty in the drift envelope is similar among the seven model combinations (Fig. 8(b)). Models M2 (f_y = 552 MPa [80 ksi]), M3 (f_y = 690 MPa [100 ksi]), and M4 (f_c' = 28 MPa [4 ksi]) generally demonstrate the highest uncertainty at low-to-moderate shaking intensities. However, at higher excitation levels, dispersion values for M2 and M3 are the lowest because a larger number of the M2 and M3 analyses approach the collapse drift limit compared to the other models.

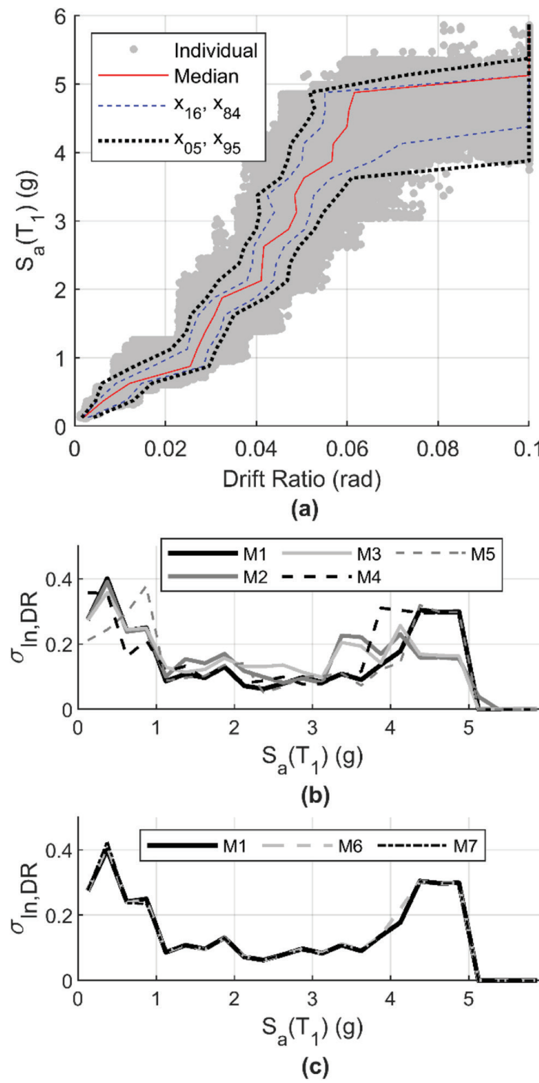

Fig. 8—(a) Model M1 drift ratio at various spectral accelerations $S_a(T_1)$*; (b) Models M1 through M5* $\sigma_{ln,DR}$ *versus* $S_a(T_1)$*; and (c) Models M1, M6, and M7* $\sigma_{ln,DR}$ *versus* $S_a(T_1)$.

Practical implementation of material uncertainty quantification

A large number of analyses are used herein to quantify the impact of variability in material properties on the seismic force-deformation response of a structure. Employing such a high number of analyses in seismic performance assessments of complex structures is impractical, especially when other sources of uncertainty are considered (for example, record-to-record uncertainty). To establish provisional recommendations for a minimum number of material samples needed to incorporate material uncertainty in seismic performance evaluations, different sample sets of the random, correlated variables in Tables 1 through 4 are generated, and nonlinear analyses are conducted to compare analytical results for the different sample sets. The sample sets differ by the sampling method—either Monte Carlo (MC) or Latin hypercube sampling (LHS)—and the number of simulations (N_{sim}). The strength of MC sampling lies in its ability to characterize the underlying distribution, thereby enabling straightforward quantification of statistical variation in the analytical results. However, MC sampling requires a large number of samples to cover outer (low probability) ranges of the distribution because samples are drawn directly from the probability density function. In contrast, LHS samples are drawn over the full range of the distribution from non-overlapping intervals of equal marginal probability, permitting smaller sample sizes.[47]

MC sample sets used herein range from N_{min} = 10 to 10,000 samples, and LHS sample sets range from N_{min} = 7 to 500 samples. The choice of N_{min} = 7 as the smallest sample set is based on the LHS method's requirement for a minimum number of samples exceeding the number of random variables ($N_{min} = N_{RV} + 1$), which results in a minimum of seven samples for M7 (N_{RV} = 6). The sample sets are drawn from truncated distributions bounded at ±2.8 standard deviations of the mean, accounting for 99.5% of the distribution. To assess the bias in a single sample, 10 unique sample sets are generated for each combination of sampling type and number.

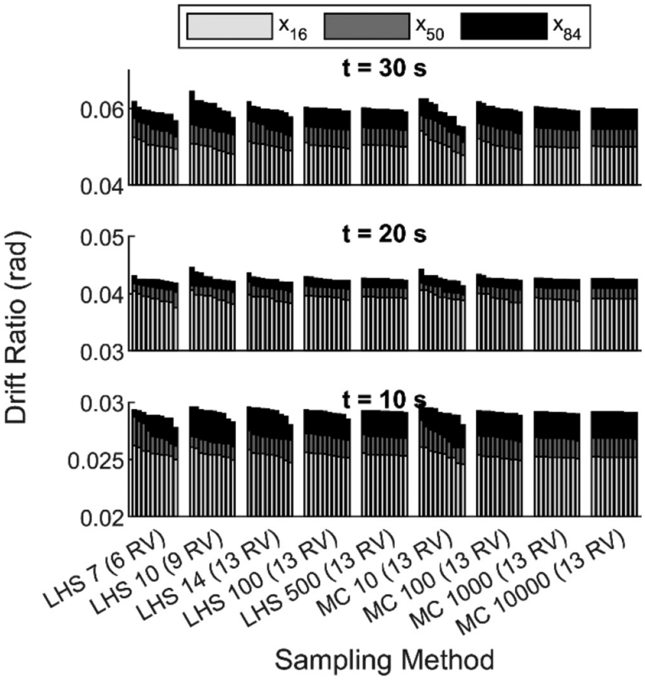

Fig. 9—Comparison of 16th, 50th, and 84th percentile drift envelope values (x_{16}, x_{50}, x_{84}) for Model M1 with different random sampling methods (10 sample sets for each method; number of random variables [RV] indicated in parentheses).

Figure 9 compares drift envelope statistical values (x_{50}, x_{16}, and x_{84}) for each sample set at three analytical time steps: t = 10, 20, and 30 seconds (refer to Fig. 7(a)). For each sampling method (for example, MC with 10,000 samples [MC 10,000]), bar plots of x_{50}, x_{16}, and x_{84} values are plotted on top of one another. Ten vertical bars are plotted for each sampling method to show the variability in x_{50}, x_{16}, and x_{84} among the 10 unique sample sets. In Fig. 9, there is no distinguishable variability in analytical results among the 10,000 MC sample sets. The COV of x_{50}, x_{16}, and x_{84} values among the 10 MC 10,000 sample sets is approximately 0.1%; thus, the use of a single 10,000 MC sample set for the material uncertainty quantification investigation reported herein is reliable and does not appear to introduce any unintentional bias to the analytical results. When a smaller number of samples is used, variability is evident among the sample sets. Sample set MC 10 has the largest COV (4.6%) among its 10 sample sets for x_{50}, x_{16}, and x_{84}. The COV among 10 sample sets for the LHS 14, LHS 10, and LHS 7 sets ranges between 1.6 and 3.2%. The results indicate that it may be reasonable to use LHS sampling with as few as $N_{sim} = N_{RV} + 1$ samples or MC sampling with as few as 10 samples to account for material uncertainty in seismic performance evaluations.

SUMMARY AND CONCLUSIONS

For performance-based seismic evaluations, the statistical variability in material properties of the structure can be used to quantify the probable range of the structure's seismic force-deformation response. In this paper, statistical distributions are developed for key material properties of ASTM A706 Grade 60, 80, and 100 reinforcing steel and normalweight concrete with specified compressive strengths between 28 and 41 MPa (4 and 6 ksi). The distributions are used to assess the importance of material property variability on the seismic force-deformation response of a validated analytical model of a reinforced concrete bridge column. It is noted that the conclusions of this paper are limited to flexural failure modes in well-confined bridge columns because the analytical model used herein does not account for flexure-shear or shear failures. Seven model combinations with different specified material properties (f_y = 414 to 690 MPa [60 to 100 ksi]; f_c' = 28 to 41 MPa [4 to 6 ksi]) and a number of uncertain material properties are considered to quantify material uncertainty. The following conclusions are drawn:

1. For the well-confined bridge column, analytical results are most sensitive to material properties that define the hardening branch of the concrete stress-strain curve (E_{cc}, f_{c0}, f_{cc}, f_t, and ε_{c0}) and the elastic branch of the reinforcing steel stress-strain curve (E_s and f_{ym}). Sensitivity to different material properties likely depends on the structure type, geometry, and detailing, as well as the analytical model type. Further research can quantify the impact of material uncertainty for other structures, including an investigation of the propagation of uncertainty to the system-level (that is, frame structure). Additional research can also evaluate uncertainty associated with the definition of the analytical model.

2. The average coefficient of variation (COV) of the column force demand is generally between 0.05 to 0.1 for all seven model combinations and does not appear to be sensitive to the specified reinforcing steel and concrete strengths.

3. The lognormal standard deviation of the column deformation response is approximately 0.1 for earthquake shaking intensities causing moderate ductility demands (for example, 1 to 5% drift ratio) and up to 0.3 for larger earthquake intensities. Larger uncertainty is observed for the model combinations with higher specified steel strength (M2 and M3) and lower specified concrete strength (M4).

4. Uncertainty in the seismic force-deformation response due to variability in material properties is reasonably estimated with as little as six random variables and seven nonlinear analyses when material properties are selected from the distributions and correlations reported herein using Latin hypercube or Monte Carlo sampling.

AUTHOR BIOS

ACI member **Christopher L. Segura Jr.** *is a Research Structural Engineer at the National Institute of Standards and Technology (NIST). He received his BS and MS from the University of Colorado Boulder, Boulder, CO, and his PhD from the University of California, Los Angeles, Los Angeles, CA. He is a member of ACI Committees 133, Disaster Reconnaissance; 369, Seismic Repair and Rehabilitation; and 374, Performance-Based Seismic Design of Concrete Buildings. His research interests include seismic design and assessment of buildings, laboratory testing, and uncertainty quantification.*

ACI member **Siamak Sattar** *is a Research Structural Engineer at NIST. He received his MS and PhD from the University of Colorado Boulder. He is Chair of ACI Subcommittees 369-C, Frames, and 374-A, Functional Recovery; and a member of ACI Committees 369, Seismic Repair and Rehabilitation; and 374, Performance-Based Seismic Design of Concrete Buildings. His research interests include seismic assessment of reinforced concrete buildings, uncertainty quantification, and functional recovery.*

Mohammad Amin Hariri-Ardebili *is a Research Associate at NIST, and an Affiliated Researcher with the University of Maryland, College Park, College Park, MD, and the University of Colorado Boulder. His research interests include uncertainty quantification, machine learning, resilience,*

risk, and performance-based earthquake engineering of infrastructures (dams, nuclear structures, bridges, and towers).

ACKNOWLEDGMENTS

The authors would like to express their gratitude to the Concrete Reinforcing Steel Institute (CRSI) for providing access to its CRSI Mill Database.

DISCLAIMER

Certain commercial software may have been used in the preparation of information contributing to this paper. Identification does not imply recommendation or endorsement by NIST, nor does it imply that such software is necessarily the best available for the purpose.

REFERENCES

1. Porter, K. A., "An Overview of PEER's Performance-Based Earthquake Engineering Methodology," *Proceedings of the Ninth International Conference on Applications of Statistics and Probability in Civil Engineering (ICASP9)*, San Francisco, CA, 2003, 8 pp.

2. Moehle, J., and Deierlein, G. G., "A Framework Methodology for Performance-Based Earthquake Engineering," *Proceedings of the 13th World Conference on Earthquake Engineering*, Vancouver, BC, Canada, 2004, 13 pp.

3. Porter, K. A.; Beck, J. L.; and Shaikhutdinov, R. V., "Sensitivity of Building Loss Estimates to Major Uncertain Variables," *Earthquake Spectra*, V. 18, No. 4, 2002, pp. 719-743. doi: 10.1193/1.1516201

4. Haselton, C. B.; Goulet, C. A.; Mitrani-Reiser, J.; Beck, J. L.; Deierlein, G. G.; Porter, K. A.; Stewart, J. P.; and Taciroglu, E., "An Assessment to Benchmark the Seismic Performance of a Code-Conforming Reinforced Concrete Moment-Frame Building," PEER Report No. 2007/12, Pacific Earthquake Engineering Research Center, Berkeley, CA, 2008, 382 pp.

5. Goulet, C. A.; Haselton, C. B.; Mitrani-Reiser, J.; Beck, J. L.; Deierlein, G. G.; Porter, K. A.; and Stewart, J. P., "Evaluation of the Seismic Performance of a Code-Conforming Reinforced-Concrete Frame Building—From Seismic Hazard to Collapse Safety and Economic Losses," *Earthquake Engineering & Structural Dynamics*, V. 36, No. 13, 2007, pp. 1973-1997. doi: 10.1002/eqe.694

6. Liel, A. B.; Haselton, C. B.; Deierlein, G. G.; and Baker, J. W., "Incorporating Modeling Uncertainties in the Assessment of Seismic Collapse Risk of Buildings," *Structural Safety*, V. 31, No. 2, 2009, pp. 197-211. doi: 10.1016/j.strusafe.2008.06.002

7. Celarec, D., and Dolšek, M., "The Impact of Modelling Uncertainties on the Seismic Performance Assessment of Reinforced Concrete Frame Buildings," *Engineering Structures*, V. 52, 2013, pp. 340-354. doi: 10.1016/j.engstruct.2013.02.036

8. Gokkaya, B. U.; Baker, J. W.; and Deierlein, G. G., "Quantifying the Impacts of Modeling Uncertainties on the Seismic Drift Demands and Collapse Risk of Buildings with Implications on Seismic Design Checks," *Earthquake Engineering & Structural Dynamics*, V. 45, No. 10, 2016, pp. 1661-1683. doi: 10.1002/eqe.2740

9. FEMA P-58-1, "Seismic Performance Assessment of Buildings, Volume 1 - Methodology," prepared by the Applied Technology Council for the Federal Emergency Management Agency, Washington, DC, 2012, 278 pp.

10. FEMA-350, "Recommended Seismic Design Criteria for New Steel Moment-Frame Buildings," prepared by the SAC Joint Venture for the Federal Emergency Management Agency, Washington, DC, 2000, 224 pp.

11. FEMA P695, "Quantification of Building Seismic Performance Factors," prepared by the Applied Technology Council for the Federal Emergency Management Agency, Washington, DC, 2009, 421 pp.

12. ASTM A706/A706M-16, "Standard Specification for Deformed and Plain Low-Alloy Steel Bars for Concrete Reinforcement," ASTM International, West Conshohocken, PA, 2016, 7 pp.

13. ACI Committee 318, "Building Code Requirements for Structural Concrete (ACI 318-19) and Commentary (ACI 318R-19)," American Concrete Institute, Farmington Hills, MI, 2019, 624 pp.

14. CRSI, "CRSI Mill Database – Annual Summary Reports for 2011-2017," Concrete Reinforcing Steel Institute, Schaumburg, IL, 2018.

15. Mirza, S. A., and MacGregor, J. G., "Variability of Mechanical Properties of Reinforcing Bars," *Journal of the Structural Division*, ASCE, V. 105, No. 5, 1979, pp. 921-937. doi: 10.1061/JSDEAG.0005146

16. Massey, F. J., Jr., "The Kolmogorov-Smirnov Test for Goodness of Fit," *Journal of the American Statistical Association*, V. 46, No. 253, 1951, pp. 68-78. doi: 10.1080/01621459.1951.10500769

17. Mander, T. J., and Matamoros, A. B., "Constitutive Modeling and Overstrength Factors for Reinforcing Steel," *ACI Structural Journal*, V. 116, No. 3, May 2019, pp. 219-232. doi: 10.14359/51713320

18. Carrillo, J.; Lozano, H.; and Arteta, C., "Mechanical Properties of Steel Reinforcing Bars for Concrete Structures in Central Colombia," *Journal of Building Engineering*, V. 33, 2021, Article No. 101858, 13 pp.

19. Spearman, C., "The Proof and Measurement of Association between Two Things," *The American Journal of Psychology*, V. 15, No. 1, 1904, pp. 72-101. doi: 10.2307/1412159

20. Sattar, S.; Weigand, J. M.; and Wong, K. K. F., "Quantification of Uncertainties in the Response of Beam-Columns in Steel Moment Frames," *Proceedings of the 11th U.S. National Conference on Earthquake Engineering*, Los Angeles, CA, 2018, 12 pp.

21. Mirza, S. A.; MacGregor, J. G.; and Hatzinikolas, M., "Statistical Descriptions of Strength of Concrete," *Journal of the Structural Division*, ASCE, V. 105, No. 6, 1979, pp. 1021-1037. doi: 10.1061/JSDEAG.0005161

22. Nowak, A. S.; Szersen, M. M.; Szeliga, E. K.; Szwed, A.; and Podhorecki, P. J., "Reliability-Based Calibration for Structural Concrete Phase 3," *Report to the Portland Cement Association and Precast/Prestressed Concrete Institute*, Skokie, IL, 2008, 115 pp.

23. ACI Committee 209, "Guide for Modeling and Calculating Shrinkage and Creep in Hardened Concrete (ACI 209.2R-08)," American Concrete Institute, Farmington Hills, MI, 2008, 45 pp.

24. Popovics, S., "A Numerical Approach to the Complete Stress-Strain Curve of Concrete," *Cement and Concrete Research*, V. 3, No. 5, 1973, pp. 583-599. doi: 10.1016/0008-8846(73)90096-3

25. Kaklauskas, G., and Ghaboussi, J., "Stress-Strain Relations for Cracked Tensile Concrete from RC Beam Tests," *Journal of Structural Engineering*, ASCE, V. 127, No. 1, 2001, pp. 64-73. doi: 10.1061/(ASCE)0733-9445(2001)127:1(64)

26. Scherbaum, F.; Bommer, J. J.; Bungum, H.; Cotton, F.; and Abrahamson, N. A., "Composite Ground-Motion Models and Logic Trees: Methodology, Sensitivities, and Uncertainties," *Bulletin of the Seismological Society of America*, V. 95, No. 5, 2005, pp. 1575-1593. doi: 10.1785/0120040229

27. Sabetta, F.; Lucantoni, A.; Bungum, H.; and Bommer, J. J., "Sensitivity of PSHA Results to Ground Motion Prediction Relations and Logic-Tree Weights," *Soil Dynamics and Earthquake Engineering*, V. 25, No. 4, 2005, pp. 317-329. doi: 10.1016/j.soildyn.2005.02.002

28. Bracchi, A.; Rota, M.; Penna, A.; and Magenes, G., "Consideration of Modelling Uncertainties in the Seismic Assessment of Masonry Buildings by Equivalent-Frame Approach," *Bulletin of Earthquake Engineering*, V. 13, No. 11, 2015, pp. 3423-3448. doi: 10.1007/s10518-015-9760-z

29. Scott, B. D.; Park, R.; and Priestley, M. J. N., "Stress-Strain Behavior of Concrete Confined by Overlapping Hoops at Low and High Strain Rates," *ACI Journal Proceedings*, V. 79, No. 1, Jan.-Feb. 1982, pp. 13-27.

30. Mander, J. B.; Priestley, M. J. N.; and Park, R., "Theoretical Stress-Strain Model for Confined Concrete," *Journal of Structural Engineering*, ASCE, V. 114, No. 8, 1988, pp. 1804-1826. doi: 10.1061/(ASCE)0733-9445(1988)114:8(1804)

31. Saatcioglu, M., and Razvi, S. R., "Strength and Ductility of Confined Concrete," *Journal of Structural Engineering*, ASCE, V. 118, No. 6, 1992, pp. 1590-1607. doi: 10.1061/(ASCE)0733-9445(1992)118:6(1590)

32. Légeron, F., and Paultre, P., "Uniaxial Confinement Model for Normal- and High-Strength Concrete Columns," *Journal of Structural Engineering*, ASCE, V. 129, No. 2, 2003, pp. 241-252. doi: 10.1061/(ASCE)0733-9445(2003)129:2(241)

33. Pauw, A., "Static Modulus of Elasticity of Concrete as Affected by Density," *ACI Journal Proceedings*, V. 57, No. 12, Dec. 1960, pp. 679-687.

34. Caltrans, "Seismic Design Criteria," California Department of Transportation, Sacramento, CA, 2006.

35. Schoettler, M. J.; Restrepo, J. I.; Guerrini, G.; Duck, D. E.; and Carrea, F., "A Full-Scale, Single-Column Bridge Bent Tested by Shake-Table Excitation," PEER Report No. 2015/02, Pacific Earthquake Engineering Research Center, Berkeley, CA, 2015, 153 pp.

36. Mazzoni, S.; McKenna, F.; and Fenves, G. L., "OpenSees Command Language Manual," University of California, Berkeley, Berkeley, CA, 2006, 465 pp.

37. Abramowitz, M., and Stegun, I. A., eds., "Handbook of Mathematical Functions with Formulas, Graphs, and Mathematical Tables," *National Bureau of Standards Applied Mathematics Series 55*, National Bureau of Standards, Washington, DC, 1964, 470 pp.

38. Chang, G. A., and Mander, J. B., "Seismic Energy Based Fatigue Damage Analysis of Bridge Columns: Part 1 – Evaluation of Seismic Capacity," *Technical Report for the National Center for Earthquake Engineering Research*, Technical Report NCEER-94-0006, State University of New York at Buffalo, Buffalo, NY, 1994, 244 pp.

39. Menegotto, M., and Pinto, P. E., "Method of Analysis of Cyclically Loaded RC Plane Frames Including Changes in Geometry and Non-Elastic Behavior of Elements Under Normal Force and Bending," *Symposium on Resistance and Ultimate Deformability of Structures Acted on by Well-Defined Repeated Loads*, Lisbon, Portugal, 1973.

40. Filippou, F. C.; Popov, E. P.; and Bertero, V. V., "Effects of Bond Deterioration on Hysteretic Behavior of Reinforced Concrete Joints," Report No. UCB/EERC-83/19, Earthquake Engineering Research Center, University of California, Berkeley, Berkeley, CA, 1983, 212 pp.

41. Coleman, J., and Spacone, E., "Localization Issues in Force-Based Frame Elements," *Journal of Structural Engineering*, ASCE, V. 127, No. 11, 2001, pp. 1257-1265. doi: 10.1061/(ASCE)0733-9445(2001)127:11(1257)

42. Estekanchi, H. E.; Valamanesh, V.; and Vafai, A., "Application of Endurance Time Method in Linear Seismic Analysis," *Engineering Structures*, V. 29, No. 10, 2007, pp. 2551-2562. doi: 10.1016/j.engstruct.2007.01.009

43. Hariri-Ardebili, M. A.; Sattar, S.; and Estekanchi, H. E., "Performance-Based Seismic Assessment of Steel Frames Using Endurance Time Analysis," *Engineering Structures*, V. 69, 2014, pp. 216-234. doi: 10.1016/j.engstruct.2014.03.019

44. Dolsek, M., "Estimation of Seismic Response Parameters Through Extended Incremental Dynamic Analysis," *Computational Methods in Earthquake Engineering*, V. 21, M. Papadrakakis, M. Fragiadakis, and N. D. Lagaros, eds., Springer, Switzerland, 2011, pp. 285-304. doi: 10.1007/978-94-007-0053-6_13

45. Caltrans, "Seismic Design Criteria Version 2.0," California Department of Transportation, Sacramento, CA, 2019, 250 pp.

46. Ibarra, L. F., and Krawinkler, H., "Global Collapse of Frame Structures under Seismic Excitations," PEER Report No. 152, Pacific Earthquake Engineering Research Center, Berkeley, CA, 2005, 301 pp.

47. Iman, R. L., and Conover, W. J., "A Distribution-Free Approach to Inducing Rank Correlation Among Input Variables," *Communications in Statistics - Simulation and Computation*, V. 11, No. 3, 1982, pp. 311-334. doi: 10.1080/03610918208812265

APPENDIX

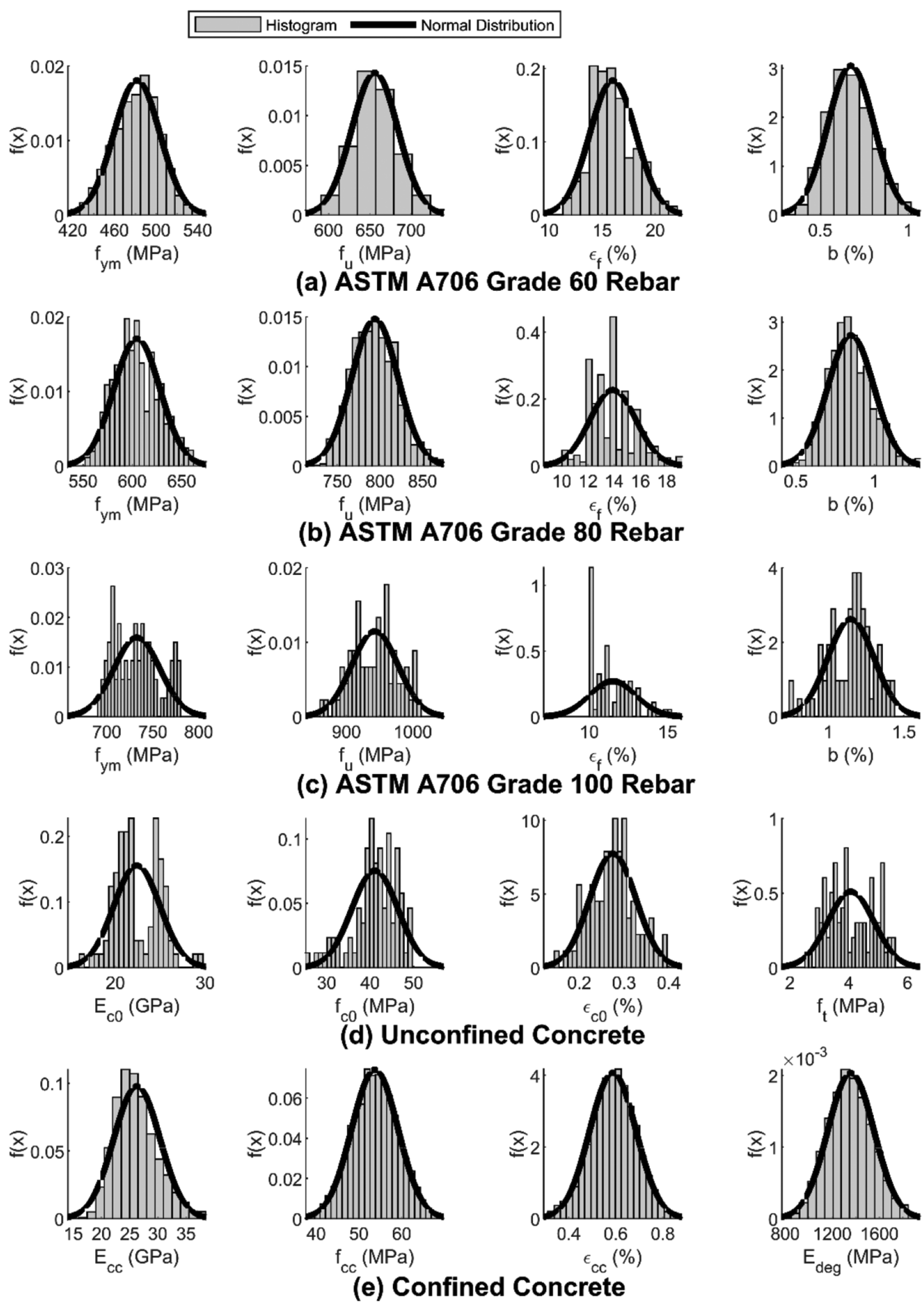

Fig. A1—Histograms for material properties with fitted normal distribution for: (a) ASTM A706 Grade 60 reinforcing bar; (b) ASTM A706 Grade 80 reinforcing bar; (c) ASTM A706 Grade 100 reinforcing bar; (d) unconfined concrete; and (e) confined concrete. (Note: 1 MPa = 0.145 ksi; 1 GPa = 145 ksi.)